

Control of microwave signals using circuit nano-electromechanics

X. Zhou,^{1,2} F. Hocke,³ A. Schliesser,^{1,2} A. Marx,³ H. Huebl,^{3,*} R. Gross,^{3,4} and T. J. Kippenberg^{1,2,†}

¹*École Polytechnique Fédérale de Lausanne (EPFL), 1015, Lausanne, Switzerland*

²*Max-Planck-Institut für Quantenoptik, 85748 Garching, Germany*

³*Walther-Meissner-Institut, 85748 Garching, Germany*

⁴*Technische Universität München, 85748 Garching, Germany*

Microwave superconducting coplanar waveguide resonators are crucial elements in sensitive astrophysical detectors [1] and circuit quantum electrodynamics (cQED) [2]. Coupled to artificial atoms in the form of superconducting qubits [3, 4], they now provide a technologically promising and scalable platform for quantum information processing tasks [2, 5–8]. Coupling these circuits, *in situ*, to other quantum systems, such as molecules [9, 10], spin ensembles [11, 12], quantum dots [13] or mechanical oscillators [14–17] has been explored to realize hybrid systems with extended functionality. Here, we couple a superconducting coplanar waveguide resonator to a nano-mechanical oscillator, and demonstrate all-microwave field controlled slowing, advancing and switching of microwave signals. This is enabled by utilizing electromechanically induced transparency [4, 5, 20], an effect analogous to electromagnetically induced transparency (EIT) in atomic physics [21]. The exquisite temporal control gained over this phenomenon provides a route towards realizing advanced protocols for storage of both classical and quantum microwave signals [22–24], extending the toolbox of quantum control techniques of the microwave field.

Cavity opto- and electro-mechanical systems [16, 17] realize parametric coupling of an electromagnetic resonance to a mechanical mode, which enables a wide range of phenomena including displacement measurements, sideband cooling or amplification of mechanical motion. In the microwave domain, this physics has been explored by coupling of superconducting cavities to micro- and nano-mechanical oscillators [14, 15, 20] enabling efficient transduction of mechanical motion with an imprecision below the level of the zero point motion [25], electro-mechanical sideband cooling to the quantum ground state [15, 26], and electromechanical amplification of microwave signals [27]. Moreover the mutual coupling of microwaves and mechanical oscillator modifies the microwave response leading to the phenomenon of electromechanically induced transparency [4]. Here we demonstrate that superconducting circuit nano-electromechanical systems enable a novel class of control phenomena over the microwave field. Exploiting the coupling of a superconducting microwave cavity to a nano-mechanical oscillator, we demonstrate tunable, sub- and superluminal microwave pulse propagation, mediated by the nano-mechanical oscillator’s response. The high mechanical quality factor enables a maximum delay of microwave pulses exceeding 3 ms, corresponding to an effective coaxial cable length of several hundreds of kilometers. Importantly, this delay is achieved with negligible losses and pulse distortion. Moreover, we explore the circuit nano-electromechanical response to a time-dependent control field, which is required for a series of advanced protocols including quantum state transfer and storage [28, 29], fast sideband cooling [30], as well as switching, modulation and routing of classical and quantum microwave signals. To this end, we demonstrate all-microwave field controlled switching and show that coun-

terintuitive regimes can be found in which the switching time can be much faster than the mechanical oscillator energy decay time. Finally, we also demonstrate mapping of the mechanical (Duffing) nonlinearity into the microwave domain.

We investigate these phenomena in a Nb superconducting circuit nano-electromechanical system (similar in geometry to the ones studied in Refs. [14, 15]) consisting of a quarter-wavelength coplanar waveguide (CPW) resonator [1] (Figure 1), parametrically coupled to a nano-mechanical oscillator, consisting of a stoichiometric, high stress Si_3N_4 beam coated with Nb. The microwave resonator studied in this work exhibits a fundamental resonance frequency of $\omega_c = 2\pi \times 6.07 \text{ GHz}$ and has a linewidth $\kappa = 2\pi \times 742 \text{ kHz}$ of which $\kappa_{\text{ex}} = \eta_c \kappa = 2\pi \times 338 \text{ kHz}$ are due to external coupling to the feed-line. The Nb/ Si_3N_4 composite nano-mechanical beam has dimensions of $60 \mu\text{m} \times 140 \text{ nm} \times 200 \text{ nm}$ and shows at cryogenic temperatures very low dissipation ($Q_m > 10^5$), with a damping rate of $\Gamma_m = 2\pi \times 12 \text{ Hz}$ resonating at $\Omega_m = 2\pi \times 1.45 \text{ MHz}$. This system thus resides in the resolved sideband regime as $\Omega_m > \kappa$. The thermal decoherence rate of the mechanical oscillator is $\Gamma_m \bar{n}_m = 2\pi \times 21 \text{ kHz}$. Here, \bar{n}_m is the thermal equilibrium phonon occupancy at the dilution refrigerator temperature of ca. 200 mK. This temperature is far below the superconducting transition temperature of Nb (9.2 K) and significantly suppresses the thermal excitation of the microwave cavity, as $\hbar\omega_c/k_B = 288 \text{ mK}$, where \hbar is the reduced Planck constant and k_B is the Boltzmann constant.

The interaction between the mechanical oscillator and the microwave coplanar waveguide resonator is formally equivalent to the optomechanical interaction [16, 17] and quantified by the vacuum coupling rate g_0 [1] in the cor-

responding interaction Hamiltonian

$$\hat{H}_{\text{int}} = \hbar g_0 (\hat{a}_m + \hat{a}_m^\dagger) \hat{n}_p \quad (1)$$

where \hat{n}_p is the intra-cavity photon number operator, and $\hat{a}_m, \hat{a}_m^\dagger$ are the ladder operators of the mechanical oscillator. The vacuum coupling rate g_0 is the product of the electro-mechanical frequency pulling parameter $G = \frac{d\omega_c}{dx}$, denoting the cavity resonance frequency change upon mechanical displacement, and the mechanical resonator's zero-point fluctuation $x_{\text{zpf}} = \sqrt{\frac{\hbar}{2m_{\text{eff}}\Omega_m}} \approx 30$ fm, where $m_{\text{eff}} \approx 7$ pg is the effective mass of the beam. The coupling rate g_0 is calibrated by applying a known frequency modulation to a microwave tone coupled into the cavity [1] (Figure 1d)). The spectrum of the homodyne readout is shown in Figure 1e) and f), yielding a measured coupling rate of $g_0 = 2\pi \times (1.26 \pm 0.05)$ Hz, independent of the microwave power reaching the coplanar waveguide cavity after several stages of attenuation in the refrigerator.

In our system, the effective radiation pressure force that is reflected by the electromechanical interaction Hamiltonian ($\hat{F} = i[\hat{H}_{\text{int}}, \hat{p}]/\hbar$), gives rise to a modification of the dynamics of the mechanical oscillator. Moreover, it leads to an interaction between two microwave fields sent simultaneously into the cavity [20, 27, 32]. This latter phenomenon which is also referred to as electromechanically induced transparency arises as the overall radiation pressure of the two fields, a strong pump at frequency ω_p and a weak probe field at frequency $\omega_p + \Omega$, drives the motion of the mechanical oscillator at the two fields' beat frequency Ω . The oscillation is resonantly enhanced if the frequency difference Ω between the two fields coincides with Ω_m . The driven motion, in turn, generates Stokes- and anti-Stokes sidebands on the pump field, which can interfere with the probe field leading to an induced transparency (or amplification for a blue detuned pump [27]). The resulting transmission coefficient of the probe field is given by

$$t_p = 1 - \frac{1}{2} \frac{1 + if(\Omega)}{-i(\bar{\Delta} + \Omega) + \kappa/2 + 2\bar{\Delta}f(\Omega)} \eta_c \kappa, \quad (2)$$

where $f(\Omega) = \hbar g_0^2 \bar{a}^2 \chi(\Omega) / (i(\bar{\Delta} - \Omega) + \kappa/2)$ and the susceptibility of the mechanical oscillator $\chi(\Omega) = m_{\text{eff}}^{-1} (\Omega_m^2 - \Omega^2 - i\Gamma_m \Omega)^{-1}$. Here, $\bar{a}^2 = \bar{n}_p = \langle \hat{n}_p \rangle$ denotes the classical expectation value of the intra-cavity pump photon number and $\bar{\Delta} = \omega_p - \omega_c + G\bar{x}$ is the effective detuning of the pump field with the static mechanical displacement \bar{x} . Figure 2 shows the measured probe transmission in the presence of a red-detuned pump $\bar{\Delta} = -\Omega_m$, resulting in an induced transmission window, which coincides with the microwave cavity resonance. The width of this window in the weak coupling regime is given by the effective damping rate $\Gamma_{\text{eff}} \approx \Gamma_m + \Gamma_{\text{dba}}$, with $\Gamma_{\text{dba}} = 4g_0^2 \bar{n}_p / \kappa$ resulting from radiation-pressure

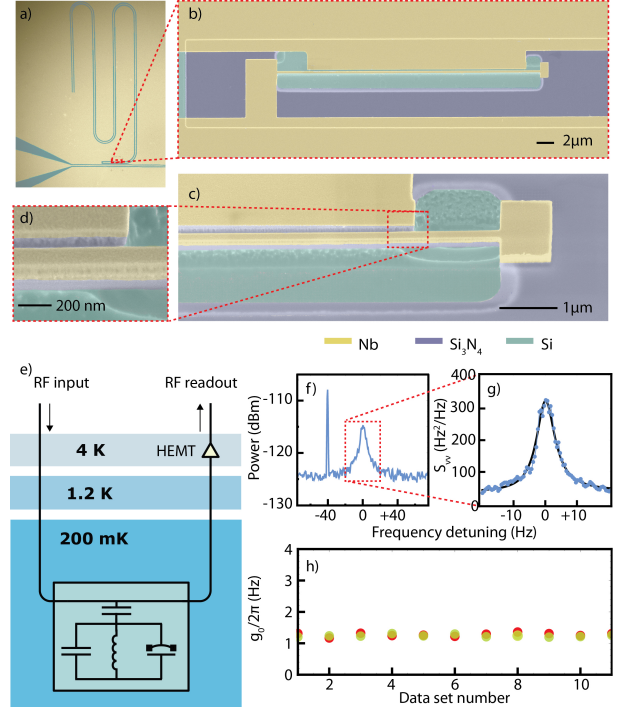


Figure 1: Superconducting circuit nano-electromechanical system. a) Falsed-colored scanning electron microscopy (SEM) of a quarter-wavelength coplanar waveguide (CPW) resonator, coupled to a CPW feedline. The Nb center stripline and ground are shown in light grey. The 6 μm gaps are patterned by etching through the Nb layer (brown) down to the Si (green). b) False-colored SEM (brown: Nb, green: Si, violet: Si₃N₄) of a 30 μm long mechanical beam integrated in the microwave cavity. Note that the beam investigated in this work is of dimensions 60 μm × 140 nm × 200 nm. c) and d) A zoomed-in view, showing the mechanical beam released from the Si substrate. e) Measurement setup with a frequency modulated pump tone on cavity resonance with $\Omega_{\text{mod}} = \Omega_m - 2\pi \times 40$ Hz and a modulation index of $2\pi \times 80$ Hz/ $\Omega_{\text{mod}} \approx 5.5 \times 10^{-5}$ as the RF input, and a homodyne RF readout after signal amplification at 4 K with a high electron mobility transistor (HEMT). f) Mechanical thermal noise spectrum and the calibration peak as measured at the Q output of the mixer. g) Calibrated frequency noise spectral density $S_{\nu\nu}$ (blue dots, $\nu \equiv \frac{\Omega}{2\pi}$) of the mechanical beam, and Lorentzian fit (black). h) The vacuum coupling rate g_0 derived from two groups (red and yellow) of measurement, with a 4 dB power difference in the modulated input tone.

induced dynamical backaction [15, 26, 33–37].

We study this response experimentally using a vector network analyzer to generate the probe tone, and analyze its direct transmission, in this case without the homodyne interferometer. A standard microwave generator provides the pump tone which is simultaneously coupled into the cavity (cf. the SI for a more detailed description of the employed measurement setup). A systematic investigation of the electromechanical effective damping as a function of pump detuning and pump intra-

cavity photon number shows excellent agreement with theory (Figure 2 a, b). Importantly, these measurements, together with the independently determined g_0 , can be used to provide an independent calibration of the intra-cavity pump photon number \bar{n}_p , and therefore the microwave attenuation in the refrigerator before entering the microwave cavity (62dB attenuation in this measurement setup).

Interestingly, the nano-electromechanical system shows significant deviations from the standard electromechanically induced transparency behavior already for moderate pump power ($\bar{n}_p = 3.9 \times 10^7$) if the probe power is increased to more than -91 dBm (Figure 2c). Strongly asymmetric lineshapes of the transmission window are observed. This asymmetry increases with an increasing probe power - much in contrast to the fully linear theory. This nonlinearity is a direct consequence of the fact that the transmission window is modified by scattering of photons induced by the mechanical oscillator. The latter exhibits a Duffing nonlinearity [2, 39] with a critical amplitude of ca. 2 nm and a Duffing parameter $\beta = 1.2 \times 10^{12} \text{ N/m}^3$, which is compatible with earlier experiments [40]. This value is independently determined in a set of measurements, in which the oscillator is driven by an externally applied low-frequency AC voltage via the DC port of a bias-tee (see SI). The full electromechanical dynamics (including the Duffing nonlinearity for $\beta \neq 0$) are captured by the set of equations in the Fourier domain :

$$A \left(-i(\Omega + \bar{\Delta}) + \frac{\kappa}{2} \right) = -i\bar{a}g_0X/x_{zpf} + \sqrt{\eta_c\kappa/2}S \quad (3)$$

$$m_{\text{eff}}(\Omega_m^2 - \Omega^2 - i\Gamma_m\Omega)X + 3\beta|X|^2X = -2\hbar A\bar{a}g_0/x_{zpf} \quad (4)$$

for the amplitude of the intra-cavity probe field A and the mechanical oscillation X . Here, the resolved-sideband regime is assumed ($\Omega_m \gg \kappa$), as well as a large mechanical quality factor $Q_m \gg \bar{a}/A$, so that that the dynamic (resonant) response of the mechanical oscillator $X \propto \bar{a}A$ is much larger than the static displacement $\bar{x} \propto \bar{a}^2$ (cf. SI). Furthermore, $|S|^2$ denotes the power of the probe field sent towards the cavity. As seen in Figure 2c, the Duffing nonlinearity is thus mapped directly onto the transmission of the probe field, yielding nonlinear behavior for probe powers as low as -91 dBm sent towards the cavity. The resulting bistability of the microwave transmission could be used for non-volatile memory applications [41].

For lower probe powers, the radiation-pressure induced oscillation amplitude of the mechanical mode remains well below the threshold for non-linear oscillations. In this regime, the transmission of the probe field is well described by equation (2). Importantly, the presence of the pump beam does not only induce a strong modifi-

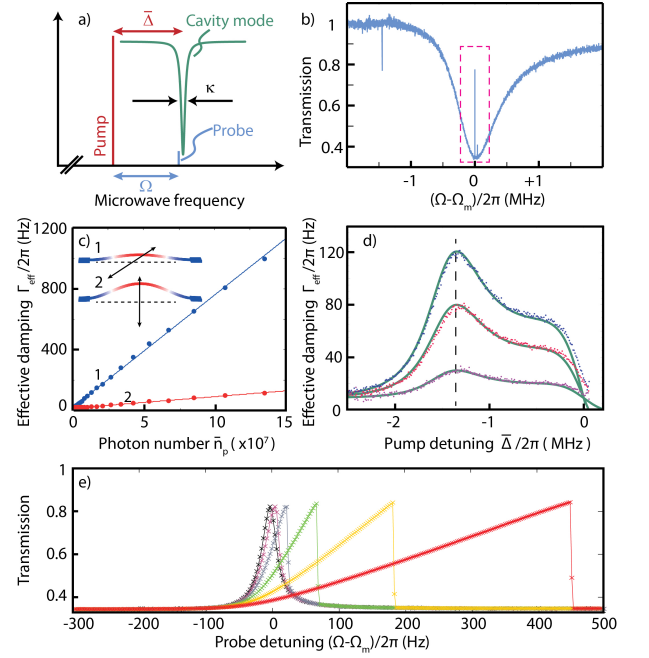


Figure 2: Electromechanical and nano-mechanical response. a) The frequency of the pump tone is detuned by $\bar{\Delta}$ from the cavity resonance frequency. The probe tone has an offset frequency Ω from the pump tone. The probe tone is tuned over the cavity resonance which has a linewidth of κ . b) The probe transmission in the presence a pump tone, as $\bar{\Delta} \approx \Omega_m$. Two transparency windows are observed, in the highlighted red rectangular, corresponding to the in-plane and out-of-plane mechanical oscillation. c) Damping rate versus intra-cavity pump photon number with pump detuning $\bar{\Delta} = -\Omega_m$ (blue: in-plane mode, red: out-of-plane mode) together with linear fits ($\Gamma_m \propto \bar{n}_p$ [34]). The probe tone has a power of -99 dBm. d) Damping rate versus pump detuning (points) and fits (lines) according to the model of dynamical backaction. The pump tone has constant powers of -57 dBm (blue), -59 dBm (red), and -64 dBm (purple), which corresponds to intra-cavity photon numbers of 1.1×10^7 , 7.2×10^6 , 2.3×10^6 at the maximum dynamical backaction damping, when the pump tone is optimally detuned ($\bar{\Delta}_{\text{opt}} = -\sqrt{\Omega_m^2 + (\kappa/2)^2}$). The probe tone has a constant power of -109 dBm. e) Electromechanically induced transparency with Duffing response. Intra-cavity pump photon number is 3.9×10^7 , powers of the probe tone are -99, -95, -91, -87, -83, and -79 dBm, respectively.

cation of the transmission of the probe field, but also leads at the same time to a fast variation of the phase $\phi = \arg(t_p)$ of the transmitted probe field across the transmission window. This can lead to significant group delays [3–6], in analogy to that achieved with the electromagnetically induced transparency in atomic [7, 8] and in solid state media [9]. The delay is given by

$$\tau_g = \frac{\partial \phi}{\partial \Omega} \quad (5)$$

for a microwave probe pulse whose center frequency falls into the transmission window. In particular,

in the resolved-sideband case and for red-detuned pumping ($\kappa < \Omega_m = -\bar{\Delta}$), the group delay is given by (see SI and [5])

$$\tau_g \approx \frac{2\eta_c C}{(1+C)(1+C-\eta_c)} \Gamma_m^{-1}, \quad (6)$$

where $C = \Omega_c^2/(\kappa\Gamma_m)$ denotes the electromechanical cooperativity parameter [47] with the coupling rate $\Omega_c = 2g_0\bar{a}$. The group delay reaches its maximum value

$$\tau_g^{\max} = 2(1 - \sqrt{1 - \eta_c})^2 / \eta_c \Gamma_m \quad (7)$$

as the cooperativity approaches $C = \sqrt{1 - \eta_c}$.

To experimentally explore this predicted behavior, microwave probe pulses are generated by modulating the amplitude of a weak (-108 dBm) probe tone derived from a microwave generator. The Gaussian-shaped envelope functions (FWHM duration 83 ms) are generated with an arbitrary waveform generator. The emission of a probe pulse is synchronized with the acquisition of the transmitted probe field. Simultaneously, a continuous-wave pump tone is sent to the cavity (see SI for details). Figure 3 shows the results of these measurements. A delay of the probe pulses can be observed when the power of the pump is varied. The maximum group delay achieved is 3.5 ms with negligible losses and pulse distortion as shown in Figure 3 a, b).

In the case of a slightly detuned probe tone, $\delta = \Omega - \Omega_m \neq 0$, a good approximation of the group delay is given by

$$\tau_g \approx -\frac{\frac{2\eta_c}{1-\eta_c} C \Gamma_m}{4\delta^2 + (1+C)^2 \Gamma_m^2} \cdot \frac{4\delta^2 - \frac{(1-\eta_c+C)(1+C)}{1-\eta_c} \Gamma_m^2}{4\delta^2 + \left(\frac{1-\eta_c+C}{1-\eta_c}\right)^2 \Gamma_m^2} \quad (8)$$

This allows for a negative group delay, i.e. the advancing of the microwave pulses, with sufficient detuning such that $|\delta| > \Gamma_m/2$. The probe delay measured when both pump tone power and probe tone detuning are varied, reveals an excellent agreement with the full theory (Figure 3 b, c, d).

For a number of advanced optomechanical protocols for both quantum and classical applications [28–30], it is necessary to dynamically tune the coupling rate

$$\Omega_c(t) = 2g_0\bar{a}(t). \quad (9)$$

For switching applications, the response of the system can be limited both by the dynamics of the mechanical mode amplitude ($X(t)$) as well as the pump field ($\bar{a}(t)$). In the following, we explore these dynamics experimentally. To this end, the pump tone is tuned to the red sideband ($\bar{\Delta} = -\Omega_m$), and switched by modulating its amplitude with rectangular pulses of $T_{\text{on}} = 150$ ms duration. The probe tone, tuned in resonance with the

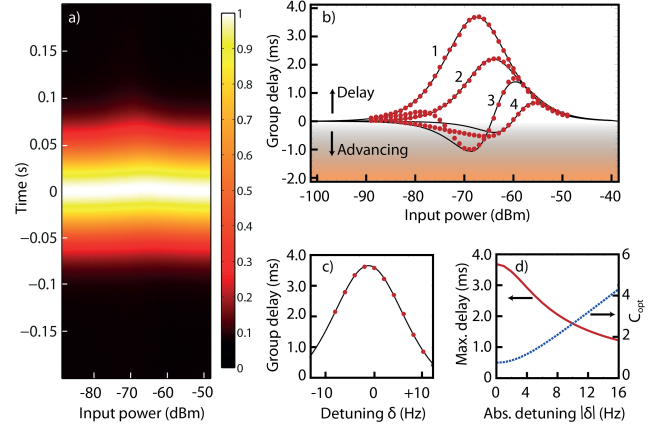


Figure 3: Sub- and superluminal microwave pulse propagation in a circuit electromechanical system in the presence of electromechanically induced transparency. a) Normalized transmitted amplitude of probe pulses, for various different pump powers between -89 dBm to -49 dBm and tuned to the red sideband, $-\bar{\Delta} = \Omega = \Omega_m$. b) Extracted group delay for pump powers between -89 dBm to -49 dBm, with various detunings $|\delta| = |\Omega - \Omega_m| = 2\pi \times (1.2 \text{ Hz}(1), 5.4 \text{ Hz}(2), 10 \text{ Hz}(3), 44 \text{ Hz}(4))$. The measured group delays - negative for superluminal and positive for subluminal propagation - are plotted (red data points) versus the input power together with the fittings from the full model (black). c) Group delay for different detunings $\bar{\Delta} + \Omega_m$ of the pump, with $\Omega = \Omega_m$ constant. The pump tone has a constant power of -66 dBm. d) Maximum delay achievable for given frequency detuning and optimum cooperativity.

cavity ($\Omega + \omega_p = \omega_c$), is constantly on, and its transmission is recorded. While the intra-cavity pump power rings up on a time scale $\kappa^{-1} \approx 0.2 \mu\text{s}$, the transmission of the probe beam builds up only at a significantly smaller rate of Γ_{eff} , at which the mechanical oscillation amplitude converges towards its steady-state value (see SI). Figure 4b) shows the characteristic timescales for probe transmission variations as a function of pump power. Upon switching off of the pump field, the probe transmission immediately drops, as the pump field (giving rise to destructive interference) decays from the resonator at a fast timescale of κ^{-1} . It is important to note that after switching off the pump and the corresponding field enhanced optomechanical coupling rate $\Omega_c(t) = 0$, the mechanical oscillation still prevails, and consequently a small fraction of the probe field is scattered to different (Stokes and anti-Stokes) frequencies. It can be shown that the modification of the transmission (with respect to the case where the coherent excitation of the mechanical oscillator's amplitude has vanished) is negligible, since in this regime the change in transmission due to the finite amplitude of the mechanical oscillator is given by $\Delta|t_p|^2/|t_p|^2 \approx \mathcal{O}(\varepsilon^2)$, with $\varepsilon = g_0 x/x_{\text{zpf}} \Omega_m$ and x being the amplitude of motion. For the amplitudes concerned in this work, ε is typically at the level

of $<1\%$. However, once the mechanical oscillation is excited to its steady state amplitude by the beating of the pump and probe fields, it decays only at a very slow rate of Γ_m in the absence of the pump beam. Therefore, advantageously for the switching, if a series of pump pulses is applied, whose period $T = T_{\text{on}} + T_{\text{off}}$ is much shorter than this timescale, the transmission of the probe follows the pump modulation, determined by the decay time κ^{-1} of the microwave cavity (Figure 4e). We show the counterintuitive regime where the switching time can be substantially faster than the slowest timescale in the problem (i.e. the inverse effective mechanical damping rate, Γ_{eff}^{-1}) and is limited only by the microwave cavities decay time ($\kappa^{-1} \ll \Gamma_{\text{eff}}^{-1}$). In a regime of intermediate pulse periods, the mechanical amplitude partially decays between the pump pulses, leading to a slower recovery of the full probe transmission when the pump is switched back on. Switching is possible if the mechanical mode does not decay significantly between the individual pump pulses ($\kappa^{-1} < T_{\text{off}} \lesssim \Gamma_m^{-1}$). During longer off-times ($T_{\text{off}} > \Gamma_m^{-1}$), the mechanical oscillator relaxes towards its equilibrium position, however $T_{\text{on}} > \Gamma_{\text{eff}}^{-1}$ suffices already to drive it back to its steady state oscillation, at which the probe tone has a transmission transparency.

Note, that while in the above electromechanical-switching experiments the pump tone is modulated, and the probe tone remains stationary, utilizing the demonstrated temporal control in conjunction with probe pulses enables to achieve storage of pump pulses in the mechanical oscillator via conversion of the pump pulse into a coherent excitation of the mechanical oscillator [23, 48].

In conclusion, we have demonstrated that electromechanically induced transparency can be used in electromechanical systems to manipulate the transmission and delay of a microwave signal in a fully integrated architecture without the need of photon detection and regeneration. Interestingly, the switching can be faster than the timescale of the mechanical oscillator's energy decay. Using electromechanically induced transparency, both classical microwave signals can be switched, or routed [49] through arrays of electromechanical systems, while the associated delays enable synchronization of microwave pulses. Both delay and advancing of pulses have been achieved. The employed microfabrication techniques offer in this context a far-reaching flexibility in the design of both mechanical and microwave properties—including carrier frequencies and bandwidth—as well as the overall architecture of complex networks. The delay and advancing of pulses may also be extended to single microwave photon pulses [5]. The prerequisites for preserving the single photon state is that the thermal decoherence time ($1/\Gamma_m \bar{n}_m$) is long compared to the photon delay/advance time. The pulse duration (i.e. bandwidth of the pulses) is limited by the width of the transparency window (Γ_{eff}) to avoid pulse distortion, implying that the condition $\Gamma_{\text{eff}} \gg \bar{n}_m \Gamma_m$ needs to be satisfied. In the

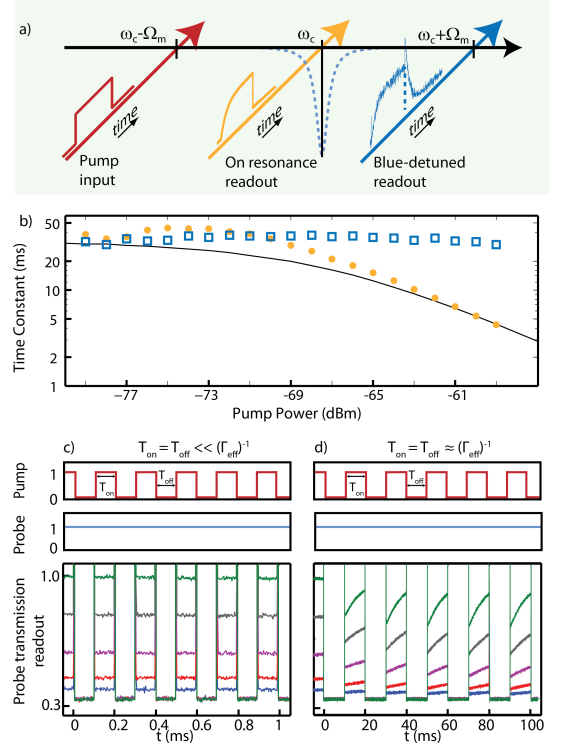


Figure 4: Switching dynamics. a) Measurement scheme, detail explained in the text. b) Time constants of the ring-up (yellow dots) and ring-down (blue squares) of the individual pulse as a function of pump power, with the pulse ring-down measured blue-detuned ($\Delta = \Omega_m$). The curve (black) shows the calculation for the ring-up constant with $\Gamma_m = 2\pi \times 12\text{ Hz}$. We expect here to have a smaller damping rate than $\Gamma_m = 2\pi \times 12\text{ Hz}$ with a lower measurement temperature here around 100 mK. c, d) A train of red-detuned ($\Delta = -\Omega_m$) pulses is sent into the cavity, with a period of $T_{\text{on}} = T_{\text{off}} = 200\text{ }\mu\text{s}$ (c) and $T_{\text{on}} = T_{\text{off}} = 20\text{ ms}$ (d), with a power descending from -63 dBm (green) to -79 dBm (blue) in steps of 4 dB. A weak probe tone (-99 dBm) is present on cavity resonance. Probe transmission on cavity resonance (ω_c) measured with a spectrum analyzer in zero span mode is plotted versus time, showing the dynamics of electromechanically induced transparency on cavity resonance.

weak coupling limit ($\Omega_c < \kappa$), the latter is equivalent to a cooperativity C exceeding the thermal occupation \bar{n}_m .

While our system already reaches coupling rates exceeding the mechanical decoherence rate $\Omega_c \gtrsim \bar{n}_m \Gamma_m$ even at a moderate cryogenic temperature, a larger g_0 [20, 28], or a simple improvement in the measurement setup, allowing a larger pump field (sustainable by the employed Nb cavities) would in principle already be sufficient for the system to reside in the coherent coupling regime $\Omega_c > (\bar{n}_m \Gamma_m, \kappa)$. Combining the system with the powerful advances in the generation and detection of single microwave photons [5], thereby may enable control over the propagation of nonclassical states using the electromechanical architecture, and allow for complete storage and retrieval of a microwave quantum state in

long-lived mechanical excitations.

Methods:

1. Nano-electromechanically coupled system: For the coplanar waveguide (CPW) structures a characteristic impedance of $Z_0 \approx 50 \Omega$ is realized with a $10 \mu\text{m}$ wide center stripline separated by a gap of $6 \mu\text{m}$ from the ground plane (see Figure 1). The one-sided cavity with a typical length of 5.3 mm is capacitively coupled to a CPW feedline on one end, and shorted on the other end. This CPW cavity is patterned into a Nb thin film deposited on top of a Si substrate. Frequency multiplexing is realized by embedding on a single chip several cavities of different length coupled to a single CPW feedline. The nano-mechanical object integrated in the cavity is a high-aspect-ratio beam, $60 \mu\text{m}$ long, 140 nm wide and has a thickness of 200 nm , which consists of 130 nm thick Nb on top of 70 nm thick tensile-stressed Si_3N_4 . The high tensile-stress of Si_3N_4 overcomes the compressive stress of Nb.

2. Low temperature measurement setup: All experiments have been performed in a dilution refrigerator at around 200 mK . In the dilution refrigerator there are three signal lines: two coaxial-cable lines connecting the two ends of the sample feedline for the microwave input- and output-signal, and a low-frequency line to carry a drive signal ($< 5 \text{ MHz}$) that enables resonant excitation of the nano-mechanical beam via Coulomb force. A sample of dimension $10 \text{ mm} \times 6 \text{ mm}$ is mounted in a gold-plated copper box. SMA coaxial connector at each end is silver-glued to the CPW feedline, transmits signals to/from the sample. Thermal noise from the tones at room temperature is suppressed using attenuators at successive temperature stages, and by the inertial attenuation of the coaxial cable. The DC-block filter besides the sample prevents the DC current in the overall transmission loop. A HEMT amplifier is anchored at 4 K and is isolated from the sample output by a circulator. For more details of the individual measurements, please refer to the SI.

Acknowledgements:

TJK acknowledges support support by the NCCR of Quantum Engineering and an ERC Starting Grant (SiMP) and the Swiss National Science Foundation (SNF). Financial support from the German Excellence Initiative via the “Nanosystems Initiative Munich” (NIM) is gratefully acknowledged. Samples were grown and fabricated at the Center of MicroNanotechnology (CMi) at EPFL. The authors acknowledge the assistance of Stefan Weis, Thomas Niemczyk and Haytham Chibani

in fabrication, Pertti Hakonen and Pasi Lahteenmaki for measurement in the early phase of the project.

Author contributions:

XZ designed and fabricated the samples. The cryogenic measurement setup was implemented by FH and HH. FH, XZ, HH and AS performed the experiments. XZ and AS performed theoretical modeling and analysis of the data. XZ wrote the paper with guidance from AS and TJK. All authors discussed the results and contributed to the final version of the manuscript.

* Electronic address: hans.huebl@wmi.badw.de

† Electronic address: tobias.kippenberg@epfl.ch

- [1] Day, P. K., LeDuc, H. G., Mazin, B. A., Vayonakis, A., and Zmuidzinas, J. *Nature* **425**(6960), 817–821 October (2003).
- [2] Wallraff, A., Schuster, D. I., Blais, A., Frunzio, L., Huang, R.-S., Majer, J., Kumar, S., Girvin, S. M., and Schoelkopf, R. J. *Nature* **431**(7005), 162–167 September (2004).
- [3] Vion, D., Aassime, A., Cottet, A., Joyez, P., Pothier, H., Urbina, C., Esteve, D., and Devoret, M. H. *Science* **296**(5569), 886–889 March (2002).
- [4] Clarke, J. and Wilhelm, F. K. *Nature* **453**(7198), 1031–1042 June (2008).
- [5] Houck, A. A., Schuster, D. I., Gambetta, J. M., Schreier, J. A., Johnson, B. R., Chow, J. M., Frunzio, L., Majer, J., Devoret, M. H., Girvin, S. M., and Schoelkopf, R. J. *Nature* **449**(7160), 328–331 September (2007).
- [6] Majer, J., Chow, J. M., Gambetta, J. M., Koch, J., Johnson, B. R., Schreier, J. A., Frunzio, L., Schuster, D. I., Houck, A. A., Wallraff, A., Blais, A., Devoret, M. H., Girvin, S. M., and Schoelkopf, R. J. *Nature* **449**(7161), 443–447 September (2007).
- [7] Schoelkopf, R. J. and Girvin, S. M. *Nature* **451**(7179), 664–669 February (2008).
- [8] Mariani, M., Wang, H., Yamamoto, T., Neeley, M., Bialczak, R. C., Chen, Y., Lenander, M., Lucero, E., O’Connell, A. D., Sank, D., Weides, M., Wenner, J., Yin, Y., Zhao, J., Korotkov, A. N., Cleland, A. N., and Martinis, J. M. *Science* **334**(6052), 61–65 July (2011).
- [9] Rabl, P., DeMille, D., Doyle, J. M., Lukin, M. D., Schoelkopf, R. J., and Zoller, P. *Physical Review Letters* **97**(3), 033003 July (2006).
- [10] Andre, A., DeMille, D., Doyle, J. M., Lukin, M. D., Maxwell, S. E., Rabl, P., Schoelkopf, R. J., and Zoller, P. *Nature Physics* **2**(9), 636–642 (2006).
- [11] Schuster, D. I., Sears, A. P., Ginossar, E., DiCarlo, L., Frunzio, L., Morton, J. J. L., Wu, H., Briggs, G. A. D., Buckley, B. B., Awschalom, D. D., and Schoelkopf, R. J. *Phys. Rev. Lett.* **105**, 140501 Sep (2010).
- [12] Kubo, Y., Grezes, C., Dewes, A., Umeda, T., Isoya, J., Sumiya, H., Morishita, N., Abe, H., Onoda, S., Ohshima, T., Jacques, V., Dreau, A., Roch, J.-F., Diniz, I., Auffeves, A., Vion, D., Esteve, D., and Bertet, P. *Phys. Rev. Lett.* **107**, 220501 Nov (2011).

- [13] Frey, T., Leek, P. J., Beck, M., Blais, A., Ihn, T., Ensslin, K., and Wallraff, A. *Physical Review Letters* **108**(4), 046807 January (2012).
- [14] Regal, C. A., Teufel, J. D., and Lehnert, K. W. *Nature Physics* **4**, 555–560 (2008).
- [15] Rocheleau, T., Ndukum, T., Macklin, C., Hertzberg, J. B., Clerk, A. A., and Schwab, K. C. *Nature* **463**(7277), 72–75 Jan (2010).
- [16] Marquardt, F. and Girvin, S. M. *Physics* **2**, 40 (2009).
- [17] Kippenberg, T. J. and Vahala, K. J. *Science* **321**, 1172–1176 (2008).
- [18] Weis, S., Rivière, R., Deléglise, S., Gavartin, E., Arcizet, O., Schliesser, A., and Kippenberg, T. J. *Science* **330**, 1520–1523 (2010).
- [19] Safavi-Naeini, A. H., Alegre, T. P. M., Chan, J., Eichenfield, M., Winger, M., Lin, Q., Hill, J. T., Chang, D. E., and Painter, O. *Nature* **472**(7341), 69–73 April (2011).
- [20] Teufel, J. D., Li, D., Allman, M. S., Cicak, K., Sirois, A. J. and Whittaker, J. D., and Simmonds, R. W. *Nature* **471** (2011).
- [21] Fleischhauer, M., Imamoglu, A., and Marangos, J. P. *Review of Modern Physics* **77**, 633–673 (2005).
- [22] Wang, Y.-D. and Clerk, A. A. *Phys. Rev. Lett.* **108**, 153603 Apr (2012).
- [23] Zhang, J., Peng, K., and Braunstein, S. L. *Phys. Rev. A* **68**, 013808 Jul (2003).
- [24] Tian, L. *Phys. Rev. Lett.* **108**, 153604 Apr (2012).
- [25] Teufel, J. D., Donner, R., Castellanos-Beltran, M. A., Harlow, J. W., and Lehnert, K. W. *Nature Nanotechnology* **4**, 820–823 (2009).
- [26] Teufel, J. D., Donner, T., Li, D., Harlow, J. W., Allman, M. S., Cicak, I. K., Sirois, A. J., Whittaker, J. D., Lehnert, K. W., and Simmonds, R. W. *Nature* **475**(7356), 359–363 July (2011).
- [27] Massel, F., Heikkilä, T. T., Pirkkalainen, J., Cho, S. U., Saloniemi, H., Hakonen, P. J., and Sillanpää, M. A. *Nature* **480**(7377), 351–354 December (2011).
- [28] Verhagen, E., Deléglise, S., Weis, S., Schliesser, A., and Kippenberg, T. J. *Nature* **482**(7383), 63–67 February (2012).
- [29] Romero-Isart, O., Pflanzner, A. C., Juan, M. L., Quidant, R., Kiesel, N., Aspelmeyer, M., and Cirac, J. I. *Physical Review Astroparticle Physics* **83**(1), 013803 Jan (2011).
- [30] Wang, X., Vinjanampathy, S., Strauch, F. W., and Jacobs, K. *Physical Review Letters* **107**(17), 177204 October (2011).
- [31] Gorodetsky, M., Schliesser, A., Anetsberger, G., Deleglise, S., and Kippenberg, T. J. *Optics Express* **18**, 23236–23246 (2010).
- [32] Agarwal, G. S. and Huang, S. *Physical Review A* **81**(4), 041803 April (2010).
- [33] Teufel, J. D., Harlow, J. D., Regal, C. A., and Lehnert, K. W. *Physical Review Letters* **101**, 197203 (2008).
- [34] Kippenberg, T. J., Rokhsari, H., Carmon, T., Scherer, A., and Vahala, K. J. *Physical Review Letters* **95**, 033901 (2005).
- [35] Schliesser, A., Del’Haye, P., Nooshi, N., Vahala, K., and Kippenberg, T. *Physical Review Letters* **97**, 243905 (2006).
- [36] Gigan, S., Böhm, H. R., Paternostro, M., Blaser, F., Langer, G., Hertzberg, J. B., Schwab, K. C., Bäuerle, D., Aspelmeyer, M., and Zeilinger, A. *Nature* **444**, 67–70 (2006).
- [37] Arcizet, O., Cohadon, P.-F., Briant, T., Pinard, M., and Heidmann, A. *Nature* **444**, 71–74 (2006).
- [38] Ali H. Nayfeh, D. T. M. *Nonlinear Oscillations*. Wiley, (1979).
- [39] Kozinsky, I., Postma, H. W. C., Bargatin, I., and Roukes, M. L. *Applied Physics Letters* **88**(25), 253101–253101–3 June (2006).
- [40] Unterreithmeier, Q. P., Faust, T., and Kotthaus, J. P. *Physical Review B* **81**(24), 241405 June (2010).
- [41] Mahboob, I. and Yamaguchi, H. *Nature Nanotechnology* **3**(5), 275–279 April (2008).
- [42] Schliesser, A. and Kippenberg, T. J. In *Advances in atomic, molecular and optical physics*, Arimondo, E., Berman, P., and Lin, C. C., editors, volume 58, chapter 5, 207–323. Elsevier Academic Press (2010).
- [43] Jiang, C., Chen, B., and Zhu, K. *EPL (Europhysics Letters)* **94**(3), 38002 May (2011).
- [44] Phillips, D. F., Fleischhauer, A., Mair, A., Walsworth, R. L., and Lukin, M. D. *Physical Review Letters* **86**, 783–786 (2001).
- [45] Liu, C., Dutton, Z., Behroozi, C., and Hau, L. *Nature* **409**, 490–493 (2001).
- [46] Longdell, J. J., Fraval, E., Sellars, M. J., and Manson, N. B. *Physical Review Letters* **95**(6), 063601 (2005).
- [47] Gröblacher, S., Hammerer, K., Vanner, M. R., and Aspelmeyer, M. *Nature* **460**, 724–727 (2009).
- [48] Fiore, V., Yang, Y., Kuzyk, M. C., Barbour, R., Tian, L., and Wang, H. *Phys. Rev. Lett.* **107**, 133601 Sep (2011).
- [49] Hoi, I., Wilson, C. M., Johansson, G., Palomaki, T., Peropadre, B., and Delsing, P. *Physical Review Letters* **107**(7), 073601 (2011).

Supplementary Information -Control of microwave signals using circuit nano-electromechanics

DETERMINATION OF THE VACUUM COUPLING RATE

The vacuum optomechanical coupling rate g_0 quantifies the strength of electromechanical coupling, analogous to cavity quantum electrodynamics. Assuming $\bar{n}_m = k_B T / \hbar \Omega_m \gg 1$ (with k_B : Boltzmann constant, T : temperature, \hbar : reduced Planck constant, Ω_m : mechanical frequency), the spectral density of fluctuations of the cavity resonance frequency induced by mechanical displacement are given by [1]

$$S_{\omega\omega}(\Omega) = G^2 S_{xx}(\Omega) \approx g_0^2 \frac{2\Omega_m}{\hbar} \frac{2\Gamma_m k_B T}{(\Omega^2 - \Omega_m^2)^2 + \Gamma_m^2 \Omega^2} \quad (\text{S1})$$

where G is the frequency pulling parameter, and Γ_m is the mechanical damping rate. The integration of equation (S1) gives

$$\langle \delta\omega_c^2 \rangle = \int_{-\infty}^{+\infty} S_{\omega\omega}(\Omega) \frac{d\Omega}{2\pi} = S_{\omega\omega}(\Omega_m) \frac{\Gamma_m \pi}{2\pi} = 2\langle \bar{n}_m \rangle g_0^2 \quad (\text{S2})$$

where \bar{n}_m is the mean mechanical occupancy. The fluctuations of the detected homodyne signal can be expressed as

$$S_{II}^{\text{meas}}(\Omega) = \frac{2K(\Omega)}{\Omega^2} S_{\omega\omega}(\Omega) \quad (\text{S3})$$

where the transduction function $K(\Omega) \equiv K(\Omega, \bar{\Delta}, \eta_c, \kappa, \bar{n}_p)$ is calibrated by applying a frequency modulation of the pump tone at frequency $\Omega_{\text{mod}} = \Omega_m - 2\pi \times 40 \text{ Hz}$, with a modulation index of $\phi_0 = 2\pi \times 80 \text{ Hz} / \Omega_{\text{mod}} \approx 5.5 \times 10^{-5}$. As the effective noise bandwidth chosen in the spectral analyzer is much narrower than the spectral features of the mechanical mode, and assuming the signal at Ω_{mod} is dominated by the modulation, the transduction function $K(\Omega)$ can then be calibrated in absolute terms at this frequency, via the relation

$$K(\Omega_{\text{mod}}) \approx 2S_{II}^{\text{meas}}(\pm\Omega_{\text{mod}}) \frac{\text{ENBW}}{\phi_0^2} \quad (\text{S4})$$

where ENBW is the bandwidth given in direct frequency, i.e. in Hz. With the homodyne detection at zero detuning ($\Delta = 0$), i.e. the pump tone ω_{pump} is on cavity resonance ω_c , in this experiment, the transduction function $K(\Omega)$ is sufficiently constant ($K(\Omega) = K(\Omega_{\text{mod}}) \approx K(\Omega_m)$) over the relevant range of frequencies. With equation (S2)-(S4), the vacuum coupling rate is derived from the measurement, knowing the mechanical occupancy number \bar{n}_m , via [1]

$$g_0^2 = \frac{1}{2\langle \bar{n}_m \rangle} \frac{\phi_0^2 \Omega_m^2}{2} \frac{S_{II}^{\text{meas}}(\Omega_m)}{S_{II}^{\text{meas}}(\pm\Omega_{\text{mod}})} \frac{\Gamma_m/4}{\text{ENBW}} \quad (\text{S5})$$

SAMPLE FABRICATION

The fabrication starts with a Si substrate (Figure S1 a)). A high tensile-stressed layer of 100 nm Si_3N_4 is deposited with low pressure chemical vapor deposition (LPCVD) on top of the Si substrate (Figure. S1 b)). Si_3N_4 is patterned into small patches using electron beam (e-beam) lithography, reactive ion etching (RIE) and buffered hydrogen fluoride (HF) etching. The mechanical beams will later sit on those patches (Figure. S1 c,d,e)). A thin Nb film of 130 nm is deposited on top of the substrate, and microwave cavities are patterned with e-beam lithography and the

Nb film is etched through with RIE (Figure. S1 f,g,h,i)). A short patch of Nb is left on top of the Si_3N_4 patch, which is between the center and ground of the MW cavity CPWs. At this exact location, the mechanical beam is patterned with e-beam lithography and released in the following fabrication steps, i.e., anisotropic- and isotropic- RIE. (Figure. S1 j,k,l))

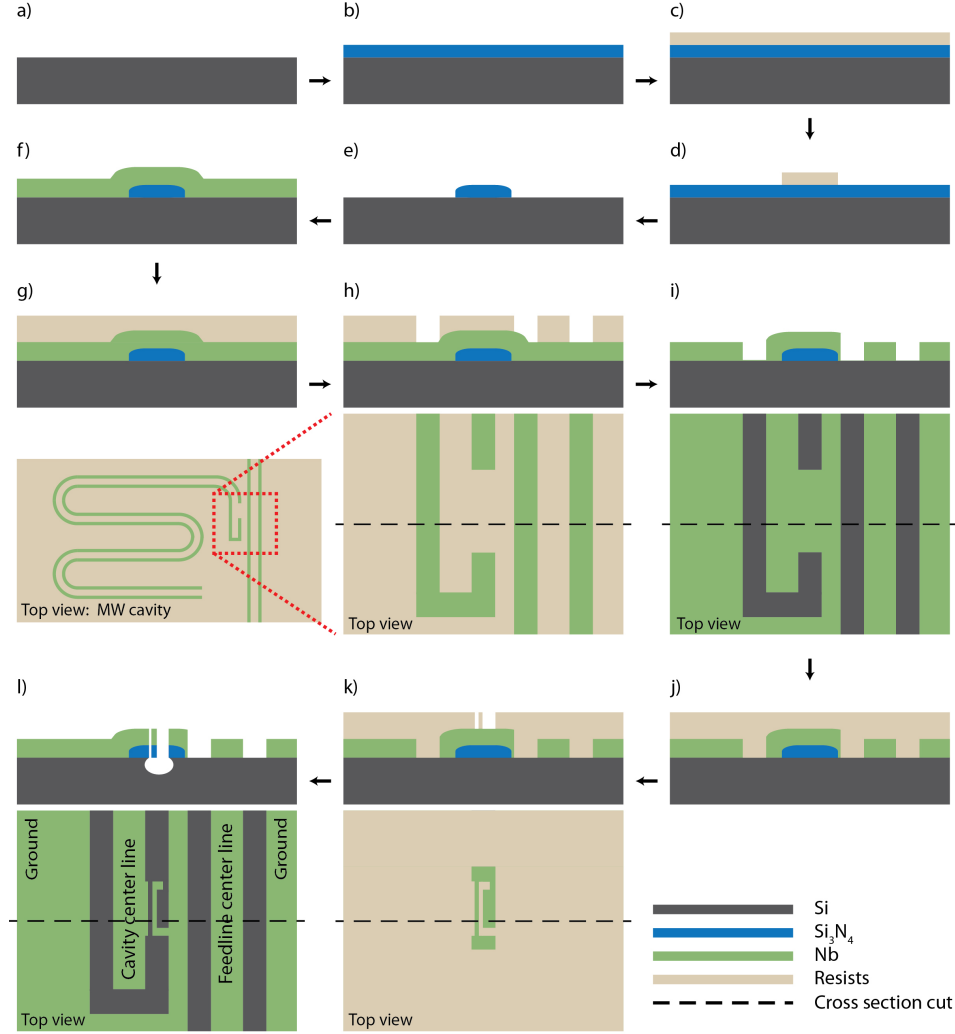


Figure S1: Fabrication flow of the electromechanical system. a) Si substrate; b) LPCVD deposition of 100nm Si_3N_4 ; c) Negative resist coating; d) E-beam patterning; e) RIE and buffered HF etching of Si_3N_4 ; f) Sputtering of 130nm Nb; g) Positive resist coating; h) E-beam patterning of MW cavities; i) RIE of Nb; j) Positive resist coating; k) E-beam patterning of mechanical beams; l) RIE of Nb, Si_3N_4 and Si.

MEASUREMENT SETUPS

The experiments are carried out at cryogenic temperature around 200 mK in a dilution refrigerator. In the dilution refrigerator there are three signal lines: two coaxial-cable lines connecting the two ends of the sample feedline for the microwave input- and output-signal, and a low-frequency line to carry a drive signal (< 5 MHz) that enables resonant excitation of the nano-mechanical beam via Coulomb force. A sample of dimension 10 mm \times 6 mm is mounted in a gold-plated copper box. SMA coaxial connectors are silver-glued to the coplanar wave guide (CPW) feedline at two ends, transmitting signals to/from the sample. Thermal noise from the tones at room temperature is suppressed using various attenuators at successive temperature stages, and by the attenuation of the coaxial cable. The DC-block filter (Minicircuits BLK-18 S+) besides the sample prevents DC currents in the overall transmission loop. A high electron mobility transistor (HEMT) amplifier is anchored to 4 K and is isolated from the sample output by a

circulator (Pamtech CTH 1392KS)).

For the OMIT measurement shown in Figure S2 a), a pump tone from a signal generator (R&S SMF 100A) and a probe tone from a network analyzer (R&S ZVA8) are coupled at room temperature and are transmitted down to the sample.

To experimentally explore the delay and advance of microwaves, as shown in Figure S2 b), a continuous-wave pump tone tuned to the red sideband ($\Delta = -\Omega_m$) is sent from a signal generator (R&S SMF 100A) to the cavity. A weak probe tone tuned in resonance ($\Omega = \Omega_m$) with the cavity is generated from a second microwave source (R&S SMF 100A). The probe tone is amplitude-modulated by a Gaussian-shaped envelope generated with an arbitrary waveform generator (LeCroy arbstudio 1104D). The emission of this pulse triggers the acquisition of the transmitted probe field via an electronic spectrum analyzer (R&S FSV-30) in zero-span mode. The actual delay of the output pulse due to the OMIT is compared to the pulse output without a pump tone present.

To study the dynamics of OMIT, the pump tone generated from a signal generator (R&S SMF 100A) is tuned to the red sideband ($\Delta = -\Omega_m$), and switched by modulating its amplitude with rectangular pulses generated from an arbitrary wave generator (LeCroy arbstudio 1104D). The probe tone generated from an independent microwave source (R&S SMF 100A), tuned in resonance with the cavity ($\Omega = \Omega_m$), is constantly on. An electronic spectrum analyzer in zero-span mode (R&S FSV-30) is triggered on with the first rectangular pulse, and the probe transmission is recorded.

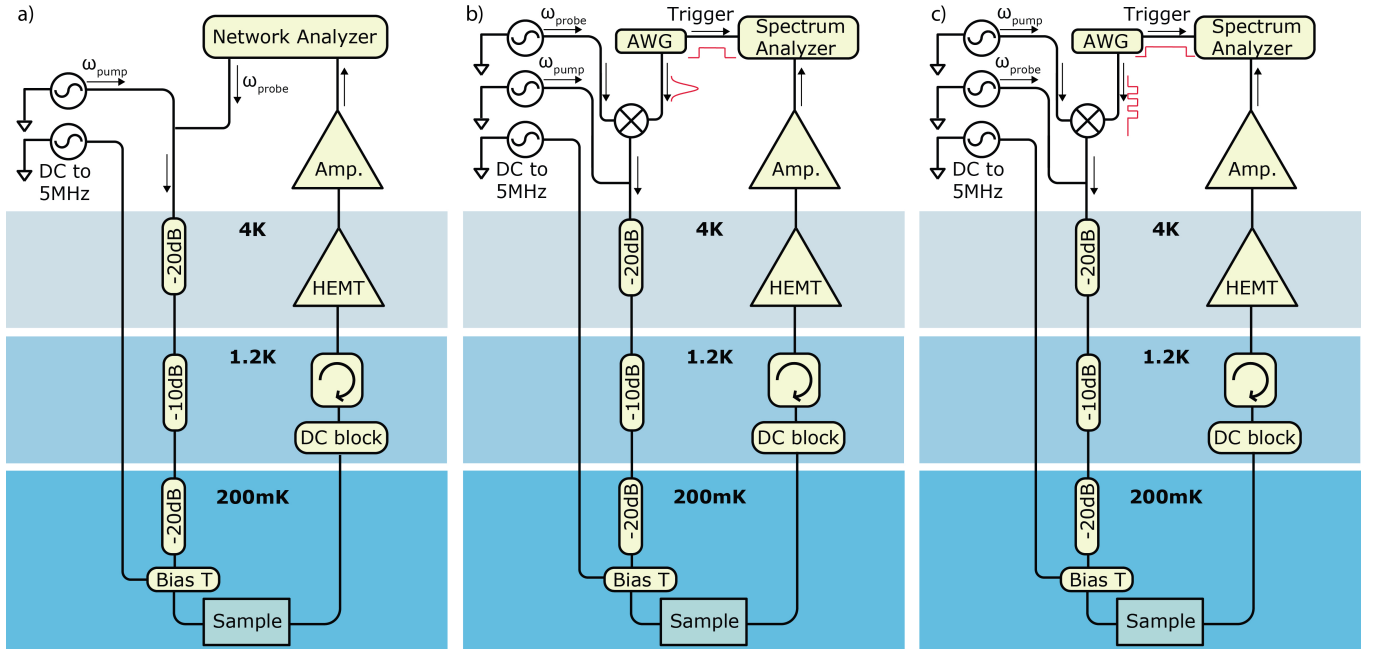


Figure S2: Measurement setups for a) OMIT, b) pulse delay measurement, and c) pulse train dynamics

MODEL FOR MECHANICAL DUFFING NONLINEARITY

In a frame rotation at the pump frequency, with $\Delta = \omega_{\text{pump}} - \omega_c$, neglecting quantum noise and thermal noise terms, we have

$$\frac{d}{dt}\hat{a}(t) = \left(i\Delta - \frac{\kappa}{2}\right)\hat{a}(t) - iG\hat{x}(t)\hat{a}(t) + \sqrt{\eta_c\kappa/2}s_{\text{in}}(t) \quad (\text{S6})$$

$$\frac{d}{dt}\hat{x}(t) = \frac{\hat{p}(t)}{m_{\text{eff}}} \quad (\text{S7})$$

$$\frac{d}{dt}\hat{p}(t) = -m_{\text{eff}}\Omega_m^2\hat{x}(t) - \hbar G\hat{a}^\dagger(t)\hat{a}(t) - \Gamma_m\hat{p}(t) - \beta\hat{x}^3(t) \quad (\text{S8})$$

where \hat{a} is the annihilation operators of the cavity mode, \hat{x} and \hat{p} are the position and momentum operators of the mechanical degree of freedom having effective mass m_{eff} and Duffing nonlinearity parameter β , and $s_{\text{in}}(t)$ is the drive amplitude normalized such that $|s_{\text{in}}(t)|^2$ is the photon flux at the input of the cavity. In the steady state, all time derivative terms are zero, and the self-consistent static solutions for intra-cavity field and mechanical displacement are:

$$\bar{a} = \frac{\sqrt{\eta_c \kappa / 2}}{-i(\Delta - G\bar{x}) + \frac{\kappa}{2}} \bar{s}_{\text{in}} \quad (\text{S } 9)$$

$$m_{\text{eff}} \Omega_m^2 \bar{x} + \beta \bar{x}^3 + \hbar G \bar{a}^2 = 0 \quad (\text{S } 10)$$

In order to solve the equations in the presence of the pump and probe fields $s_{\text{in}}(t) = \bar{s}_{\text{in}} + \delta s_{\text{in}}(t)$, we use the ansatz $\hat{a}(t) = \bar{a} + \delta \hat{a}(t)$, $\hat{x}(t) = \bar{x} + \delta \hat{x}(t)$, and chose the phase reference of the cavity field so that \bar{a} is real and positive. Then we have

$$\frac{d}{dt} \delta \hat{a}(t) = \left(i\Delta - iG\bar{x} - \frac{\kappa}{2} \right) \delta \hat{a} - iG(\bar{a} + \hat{a}(t)) \delta \hat{x}(t) + \sqrt{\eta_c \kappa / 2} \delta s_{\text{in}}(t) \quad (\text{S } 11)$$

$$m_{\text{eff}} \left(\frac{d^2}{dt^2} \delta \hat{x}(t) + \Gamma_m \frac{d}{dt} \delta \hat{x}(t) + \Omega_m^2 \delta \hat{x}(t) \right) = -\hbar G \bar{a} (\delta \hat{a}(t) + \delta \hat{a}^\dagger(t)) - \beta (\bar{x}^3 + \delta \hat{x}^3(t) + 3\bar{x}^2 \delta \hat{x}(t) + 3\bar{x} \delta \hat{x}^2(t)) \quad (\text{S } 12)$$

For a given $\Omega = \omega_{\text{probe}} - \omega_{\text{pump}}$, and a probe field of $\delta s_{\text{in}}(t) = s_P e^{-i\Omega t}$, we furthermore use the ansatz for the sideband fields of the pump (one of which is the probe):

$$\delta a(t) = A^- e^{-i\Omega t} + A^+ e^{+i\Omega t} \quad (\text{S } 13)$$

$$\delta a^*(t) = (A^+)^* e^{-i\Omega t} + (A^-)^* e^{+i\Omega t} \quad (\text{S } 14)$$

$$\delta x(t) = X e^{-i\Omega t} + X^* e^{+i\Omega t} \quad (\text{S } 15)$$

Sorting the rotation terms, the relevant equations with $e^{-i\Omega t}$ are given by

$$A^- \left(-i(\Omega + \Delta + G\bar{x}) + \frac{\kappa}{2} \right) = -iG\bar{a}X + \sqrt{\eta_c \kappa / 2} s_P \quad (\text{S } 16)$$

$$A^+ \left(i(\Omega - \Delta - G\bar{x}) + \frac{\kappa}{2} \right) = -iG\bar{a}X^* \quad (\text{S } 17)$$

$$m_{\text{eff}} (\Omega_m^2 - \Omega^2 - i\Gamma_m \Omega) X = -\hbar G \bar{a} (A^- + (A^+)^*) - 3\beta (\bar{x}^2 X + |X|^2 X) \quad (\text{S } 18)$$

In the resolved side band regime, the lower sideband A^+ is far off-resonance and is much smaller than A^- , we therefore write $A \approx A^-$ and approximate $A^+ \approx 0$. Here, the resolved-sideband regime is assumed ($\Omega_m \gg \kappa$), as well as a large mechanical quality factor $\Omega_m / \Gamma_m \gg \bar{a} / A$, so that the dynamic (resonant) response of the mechanical oscillator $X \propto \bar{a} A$ is much larger than the static displacement $\bar{x} \propto \bar{a}^2$. Taking into account that $\bar{x} \ll \delta \hat{x}(t)$, and using $\bar{\Delta} = \Delta + G\bar{x}$ where $G = g_0 / \sqrt{\frac{\hbar}{2m_{\text{eff}}\Omega_m}}$, we have the pair of equations in the main article:

$$A \left(-i(\Omega + \bar{\Delta}) + \frac{\kappa}{2} \right) = -i\bar{a}g_0 \sqrt{\frac{2m_{\text{eff}}\Omega_m}{\hbar}} X + \sqrt{\eta_c \kappa / 2} s_P \quad (\text{S } 19)$$

$$m_{\text{eff}} (\Omega_m^2 - \Omega^2 - i\Gamma_m \Omega) X + 3\beta |X|^2 X = -2A\bar{a}g_0 \sqrt{2\Omega_m \hbar m_{\text{eff}}} \quad (\text{S } 20)$$

The transmission ratio of the probe field is given by:

$$t_P = \frac{s_P - \sqrt{\eta_c \kappa / 2} A}{s_P} \quad (\text{S } 21)$$

An independent calibration measurement of the Duffing parameter β is carried out by a direct mechanical driving through the low-frequency line coupled to the cavity via a bias-T. A vector network analyzer centered around the mechanical frequency Ω_m probes over a 200 Hz wide spectrum. A probe tone of $\omega = \omega_c$ is sent simultaneously into the cavity with a frequency modulation at $\Omega_{\text{mod}} = \Omega_m - 2\pi \times 80 \text{ Hz}$ and a modulation index of $2\pi \times 100 \text{ kHz} / \Omega_{\text{mod}}$. The frequency modulation from the driven mechanical oscillation is calibrated with this injected frequency modulation,

from the homodyne readout spectrum in Figure S3. The amplitude of the mechanical displacement is given by

$$x = \frac{S_{II}^{\text{meas}}(\Omega_m)}{S_{II}^{\text{meas}}(\Omega_{\text{mod}})} (\Omega_m \phi_0) \frac{x_{\text{zpf}}}{g_0} \quad (\text{S } 22)$$

From these measurements, the critical displacement $x_c = 2.2 \text{ nm}$ and the Duffing parameter $\beta = 1.6 \times 10^{12} \text{ N/m}^3$ can be calculated[2].

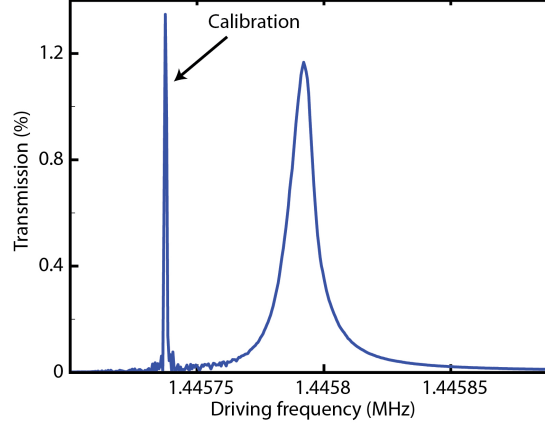


Figure S3: Homodyne readout spectrum of the driven mechanical oscillation and the frequency modulation calibration.

THEORY OF SLOWING MICROWAVE

The presence of the pump beam does not only induce a strong modification of the transmission of the probe field, and at the same time leads to a fast variation of the phase of the transmitted probe field across the transmission window

$$\phi = \arg(t_p) \quad (\text{S } 23)$$

This can lead to significant group delays [3–6], analog to that achieved with the electromagnetically induced transparency in atomic [7, 8] and in solid state media [9].

$$\tau_g = \frac{\partial \phi}{\partial \Omega} \quad (\text{S } 24)$$

In the case of red-detuned pumping ($\bar{\Delta} = -\Omega_m$) and $\Omega = \Omega_m$, the group delay is approximated as,

$$\tau_g = \frac{2\eta_c C}{(1 + C - \eta)(1 + C)} \Gamma_m^{-1} \quad (\text{S } 25)$$

assuming only the mechanical susceptibility contributes to the phase of the transmission spectrum ($\Gamma_{\text{eff}} \ll \kappa$). Here $C = (2g_0\bar{a})^2/(\kappa\Gamma_m)$ denotes the optomechanical cooperativity parameter, and η_c is cavity coupling parameter defined as the ratio of the cavity coupling rate to the cavity damping rate ($\eta_c = \kappa_{\text{ex}}/\kappa$). The maximum group delay is reached when

$$\frac{\partial}{\partial C} \tau_g \equiv 0 \quad (\text{S } 26)$$

The maximum group delay is given by

$$\tau_g^{\max} = 2(1 - \sqrt{1 - \eta_c})^2 / \eta_c \Gamma_m \quad (\text{S } 27)$$

when the cooperativity approaches $C = \sqrt{1 - \eta_c}$.

In the case with a slightly detuned probe tone, $\delta = \Omega - \Omega_m$, a good approximation of the group delay is given by

$$\tau_g \approx -\frac{\frac{2\eta_c}{1-\eta_c} C \Gamma_m}{4\delta^2 + (1+C)^2 \Gamma_m^2} \cdot \frac{4\delta^2 - \frac{(1-\eta_c+C)(1+C)}{1-\eta_c} \Gamma_m^2}{4\delta^2 + \left(\frac{1-\eta_c+C}{1-\eta_c}\right)^2 \Gamma_m^2} \quad (\text{S } 28)$$

This equation allows the group delay to be negative, i.e. the advancing of the microwave waveforms, as long as the condition of $|\delta| > \Gamma_m/2$ is met.

The pulse delay is limited by the bandwidth of the transparency window ($\Delta\nu \sim \Gamma_{\text{eff}}/2\pi$), as the medium becomes increasingly opaque at frequencies outside the transparency window, resulting in spreading of the pulse. In order to preserve the pulse, the Gaussian pulse bandwidth should be smaller than the bandwidth of the transmission window ($\text{BW}_p < \Delta\nu$). In the main test, we study the group delay of a pulse with a full-width-half-maximum (FWHM) duration of 83ms, which satisfies this condition. To study the pulse distortion, a Gaussian pulse of 17ms FWHM is sent to the cavity as a probe, and readout with a spectrum analyzer. As shown in Figure S4, the distortion reaches its maximum at the largest group delay.

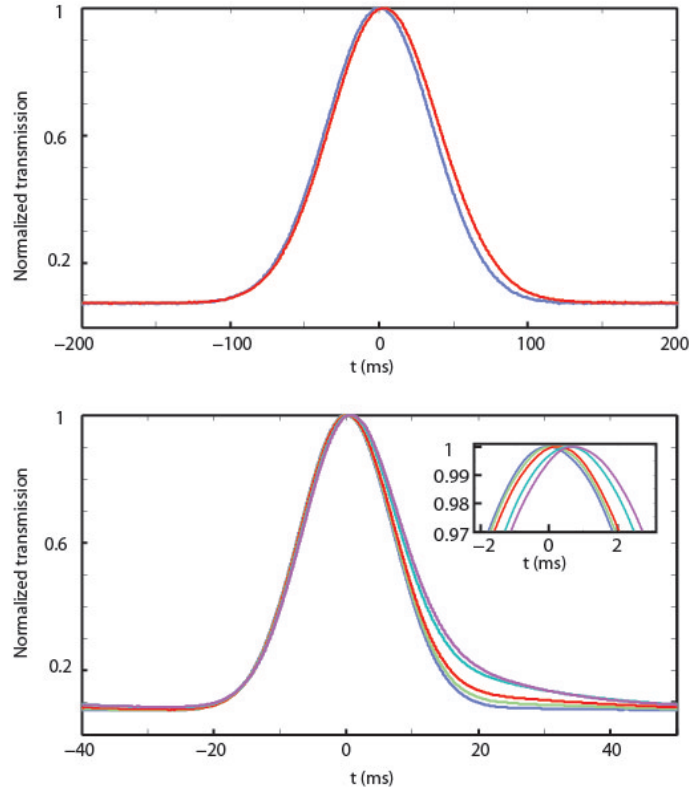


Figure S4: Pulse delays and distortions. a) The non-delayed (blue) and delayed (red) Gaussian pulses with FWHM of 83ms. b) The non-delayed and delayed pulses with FWHM of 17ms.

THEORY OF DYNAMICAL SWITCHING OF OPTOMECHANICALLY INDUCED TRANSPARENCY

We study the switching dynamics in a frame rotating at the pump frequency ω_{pump} . We have the following set of ansatz

$$\delta a(t) = A^-(t)e^{-i\Omega t} + A^+(t)e^{+i\Omega t} \quad (\text{S } 29)$$

$$\delta a^*(t) = (A^+(t))^* e^{-i\Omega t} + (A^-(t))^* e^{+i\Omega t} \quad (\text{S } 30)$$

$$\delta x(t) = X(t)e^{-i\Omega t} + X(t)^* e^{+i\Omega t} \quad (\text{S } 31)$$

The intra-cavity field $\bar{a}(t)$ has a fast converge to its steady-state value \bar{a} (either \bar{a}_{on} or \bar{a}_{off}) at a rate of $\kappa/2$. Applying the set of ansetz to equation (S 11)(S 12), and sort by rotation terms, the relevant equations with $e^{-i\Omega t}$ are

$$\begin{aligned} \frac{d}{dt}A^-(t) &= \left(i(\Omega + \bar{\Delta}) - \frac{\kappa}{2}\right) A^-(t) - iG\bar{a}X(t) + \sqrt{\eta_c\kappa/2}s_P \\ \frac{d}{dt}A^+(t)^* &= \left(i(\Omega - \bar{\Delta}) - \frac{\kappa}{2}\right) (A^+(t))^* + iG\bar{a}X(t)^* \\ \frac{d^2}{dt^2}X(t) + \frac{d}{dt}X(t)(\Gamma_m - 2i\Omega) + (\Omega_m^2 - \Omega^2 - i\Gamma_m\Omega)X(t) &= -m_{\text{eff}}^{-1}\hbar G\bar{a}(t) \left(A^-(t) + (A^+(t))^*\right) \end{aligned} \quad (\text{S } 32)$$

Note that we have assumed small excitation amplitudes so that the Duffing nonlinearity is negligible. Due to the low mechanical damping rate, we assume a the very slowing varying envelope of the displacement of the mechanical oscillator, $\frac{d^2}{dt^2}X(t) \ll \Omega \frac{d}{dt}X(t)$, $\Gamma_m \frac{d}{dt}X(t) \ll \Omega \frac{d}{dt}X(t)$ with $\Omega \approx \Omega_m$. Further in the resolved-sideband regime, $A^+(t) \approx 0$. The cavity field amplitude $A(t)$ varies slowly as well, and therefore we have $|\frac{d}{dt}A(t)| \ll |\frac{\kappa}{2}A(t)|$. The set of equations (S 32) can then be simplified as

$$\begin{aligned} 0 &= i\left(\Omega + \bar{\Delta} - \frac{\kappa}{2}\right) (A^-(t))^* - iG\bar{a}X(t) + \sqrt{\eta_c\kappa/2}s_P \\ A^+(t) &= 0 \\ \frac{d}{dt}X(t)(-2i\Omega) + (\Omega_m^2 - \Omega^2 - i\Gamma_m\Omega)X(t) &= -m_{\text{eff}}^{-1}\hbar G\bar{a}A(t) \end{aligned} \quad (\text{S } 33)$$

the solution of $A(t) \approx A^-(t)$ with detunning $-\bar{\Delta} = \Omega = \Omega_m$ is approximately given by

$$A(t) = \frac{-iGX(t)\bar{a} + \sqrt{\eta_c\kappa/2}s_P}{\kappa/2} \quad (\text{S } 34)$$

Note the temporal dynamics of the amplitude $A(t)$ is only determined by the temporal dynamics of the mechanical displacement amplitude $X(t)$. Using this solution in the equation of motion for $X(t)$, we have

$$\frac{d}{dt}X(t) = -\left(\frac{\Gamma_m}{2} + \frac{2\bar{a}^2G^2}{\kappa}x_{\text{zpf}}^2\right)X(t) - iG\bar{a}x_{\text{zpf}}^2\left(\frac{\sqrt{\eta_c\kappa/2}s_P}{\kappa/2}\right) \quad (\text{S } 35)$$

Switch-on dynamics

Without loss of generality, we assume that at the time $t = 0$ the pump tone is injected into the cavity $P_{\text{in}}(t) = P_{\text{in}}[\text{sgn}(t) + 1]$ and the initial mechanical oscillation amplitude $X(0) = 0$, the solution of equation (S 35) has the form

$$X(t) = X_{ss} \left(1 - e^{-\frac{\Gamma_{\text{eff}}}{2}t}\right) \quad (\text{S } 36)$$

where $X_{ss} = X(t \rightarrow \infty) = -iG\bar{a}_{\text{on}}x_{\text{zpf}}^2\left(\frac{\sqrt{\eta_c\kappa/2}s_P}{\kappa/2}\right)$ is its steady-state amplitude. Physically this means that $X(t)$ rings up to its steady-state amplitude X at a rate $\Gamma_{\text{eff}} = \frac{\Gamma_m}{2} + \frac{2\bar{a}_{\text{on}}^2G^2}{\kappa}x_{\text{zpf}}^2$. The solution of $A(t)$ is then given by

$$A(t) = \frac{-iGX_{ss}\left(1 - e^{-\frac{\Gamma_{\text{eff}}}{2}t}\right)\bar{a}_{\text{on}} + \sqrt{\eta_c\kappa/2}s_P}{\kappa/2} \quad (\text{S } 37)$$

having the initial amplitude $A(0) = \frac{\sqrt{\eta_c\kappa/2}s_P}{\kappa/2}$, and the steady state amplitude $A_{ss} = A(t \rightarrow \infty) = \frac{-iGX_{ss}\bar{a}_{\text{on}} + \sqrt{\eta_c\kappa/2}s_P}{\kappa/2}$. This implies that the intra-cavity amplitude $A(t)$ rings down at a rate close to $\Gamma_{\text{eff}}/2$ and reaches its steady state amplitude A_{ss} . The readout of the transmitted field $t_p = 1 - \sqrt{\eta_c\kappa/2}A(t)/s_P$, therefore, rings up at a rate close to $\Gamma_{\text{eff}}/2$, as shown in Figure S5.

Switch-off dynamics

Moreover, when the pump field is switched off, the intra-cavity photon from the pump $\bar{a}(t)$ decays to $\bar{a}_{\text{off}} \approx 0$ at a fast rate of $\kappa/2$, resulting in a fast increase of the intra-cavity field to $A(t)|_{\text{pump-off}} = \frac{\sqrt{\eta_c \kappa/2 s_P}}{\kappa/2}$, corresponding to a fast decay of transmission amplitude t_p shown in Fig.S5a) at $t = 150$ ms. Due to the absence of the pump tone ($\bar{a}=0$), and further with $X(t)|_{\text{pump-off}} = X_{ss}$, the mechanical oscillation amplitude (S 35) decays, in this case, as

$$X(t) = X_{ss} e^{-\frac{\Gamma_m}{2} t} \quad (\text{S } 38)$$

A qualitative measure of this decay is given by the Raman-scattered field amplitude $B_0(t)$ at the blue sideband of the cavity (i.e. $\omega_c + \Omega_m$), to which the mechanical oscillation scatters part of the probe light even in absence of the pump. As $B_0(t)$ is proportional to $\left(-\frac{\sqrt{\eta_c \kappa/2 s_P}}{\kappa/2}\right) X(t)$, the scattered field $B_0(t)$ rings down at a rate of $\Gamma_m/2$, as shown in Figure S5 b). The strong initial rise is associated with the fast rise of the intra-cavity probe amplitude to $A(t)|_{\text{pump-off}}$ as the pump field is switched off.

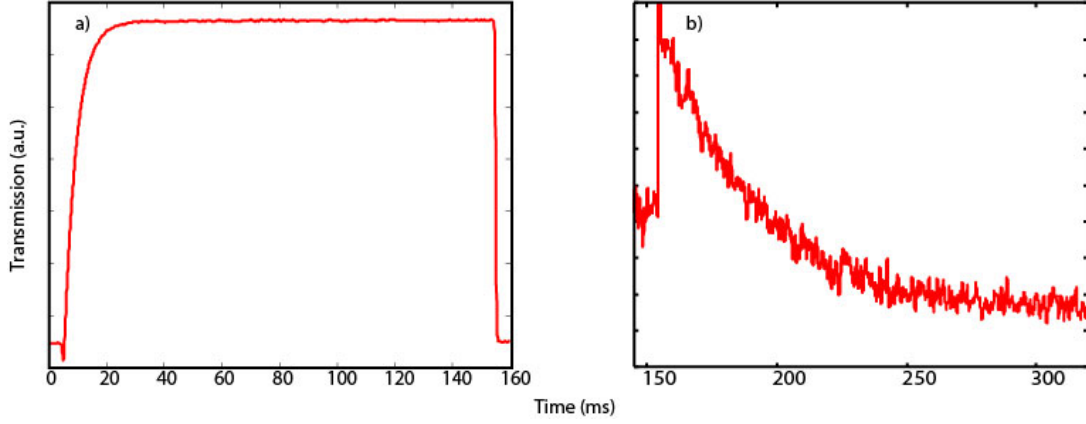


Figure S5: Probe field transmission t_p . a) Probe on cavity resonance (ω_c). The probe transmission rings up at the rate of $\Gamma_{\text{eff}}/2$ upon switching on the pump tone. The probe transmission immediately drops at $T=150$ ms as pump tone switches off. b) Probe blue-detuned to the cavity ($\omega_c + \Omega_m$). The probe transmission increases at a fast rate ($\kappa/2$) upon switching off of the pump tone, and follows by a decay at a rate of $\Gamma_m/2$.

* Electronic address: hans.huebl@wmi.badw.de

† Electronic address: tobias.kippenberg@epfl.ch

- [1] Gorodetsky, M., Schliesser, A., Anetsberger, G., Deleglise, S., and Kippenberg, T. J. *Optics Express* **18**, 23236–23246 (2010).
- [2] Ali H. Nayfeh, D. T. M. *Nonlinear Oscillations*. Wiley, (1979).
- [3] Schliesser, A. and Kippenberg, T. J. In *Advances in atomic, molecular and optical physics*, Arimondo, E., Berman, P., and Lin, C. C., editors, volume 58, chapter 5, 207–323. Elsevier Academic Press (2010).
- [4] Weis, S., Rivière, R., Deléglise, S., Gavartin, E., Arcizet, O., Schliesser, A., and Kippenberg, T. J. *Science* **330**, 1520–1523 (2010).
- [5] Safavi-Naeini, A. H., Alegre, T. P. M., Chan, J., Eichenfield, M., Winger, M., Lin, Q., Hill, J. T., Chang, D. E., and Painter, O. *Nature* **472**(7341), 69–73 April (2011).
- [6] Jiang, C., Chen, B., and Zhu, K. *EPL (Europhysics Letters)* **94**(3), 38002 May (2011).
- [7] Phillips, D. F., Fleischhauer, A., Mair, A., Walsworth, R. L., and Lukin, M. D. *Physical Review Letters* **86**, 783–786 (2001).
- [8] Liu, C., Dutton, Z., Behroozi, C., and Hau, L. *Nature* **409**, 490–493 (2001).
- [9] Longdell, J. J., Fraval, E., Sellars, M. J., and Manson, N. B. *Physical Review Letters* **95**(6), 063601 (2005).